Narrow Graphene Nanoribbons from Carbon Nanotubes

Liying Jiao*, Li Zhang*, Xinran Wang & Hongjie Dai†

Department of Chemistry and Laboratory for Advanced Materials, Stanford University, Stanford, California 94305, USA

** These authors contributed equally to this work*

Supplementary Information

(1) Histograms of pristine MWNTs and GNRs

(2) Yield of single and few-layer GNRs

(3) Raman spectra of GNRs

(4) Raman spectra of pristine MWNTs

(5) Choice of plasma source and etching parameters

(6) Transfer properties of more GNR device

(1) Histograms of pristine MWNTs and GNRs

We measured the diameter of more than 100 MWNTs (Bucky tube, Aldrich) on Si substrate with AFM. Figure S1a showed the diameter distribution of pristine MWNTs. The distribution of diameters ranged from 4 to 18 nm and the mean diameter was ~8 nm. Because of the difficulties of distinguishing multi-layer GNRs from GNRs with CNTs cores by AFM, we only measured the widths and heights of single or few-layer GNRs (height < 2 nm). As shown in Fig. S1b, the widths of most GNRs were in the range of 10 to 20 nm. The heights of GNRs distributed around three discrete values, i.e. ~0.8 nm, 1.3 nm and 1.8 nm (Fig. S1c), which were assigned to single, bi- and tri-layer GNRs, respectively. Most GNRs we obtained were single and bi-layer.

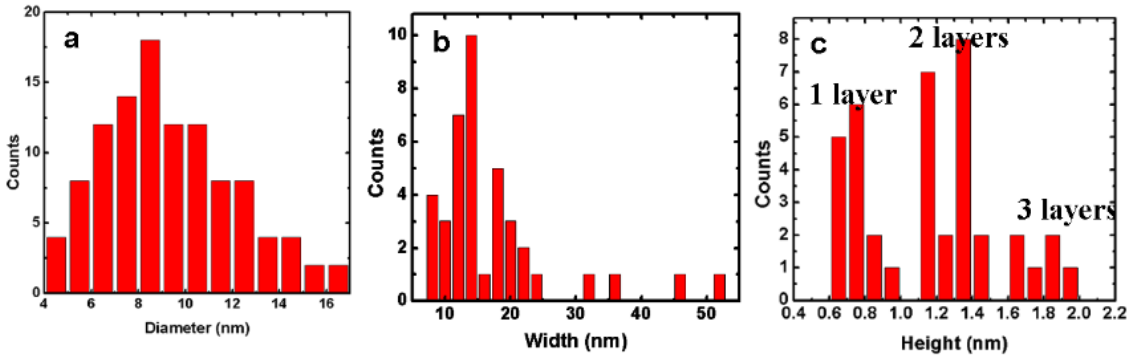

Figure S1 a, Diameter distribution of pristine MWNTs. **b** and **c**, histogram of width and height distributions of GNRs generated by unzipping MWNTs.

(2) Yield of single and few-layer GNRs

The yield of single and few-layer GNRs was determined by the diameter, number of shells of the starting MWNTs and the etching time. In this work, the yield of GNRs with high quality was ~20% after etching for 10 s. By assuming that the width of GNRs was comparable with half of the circumference of the starting MWNTs, we estimated that GNRs with a width of 10-20 nm were converted from MWNTs with a diameter of 6-12 nm. From the diameter distribution of MWNTs (Fig. S1a) ~40% of pristine MWNTs had a diameter of 6-12 nm. However, the number of shells of MWNTs varied even with the same diameter and only few-walled CNTs could generate single or few-layer GNRs. Therefore, the yield of single and few-layer GNRs was much lower than 40%.

(3) Raman spectra of GNRs

The phonon energies and the Raman shift observed for 2D band depend on the electronic structure of the graphene films. The 2D line shape of single layer graphene is composed of one Lorentzian peak. For AB-stacked bi-layer graphene, the strong interaction between the two layers splits the degenerate electronic conduction (and valence) bands, giving rise to four Lorentzian components in the 2D peak. For non-AB-stacked structures, the interaction between the two layers is weak and the 2D peak remains as a single Lorentzian peak[2,3]. Figure S2 showed a typical Raman spectrum of a non-AB-stacked bi-layer GNR observed in our experiments. The full width of half maximum (FWHM) of the 2D band of this GNR was ~48 cm^{-1}, much wider than the 2D peak of single layer

GNRs (FWHM~38 cm^{-1}). Figure S3 showed a typical Raman spectrum of a tri-layer GNR. The 2D band could be fitted with two Lorentzian peaks, characteristic of few-layer ABA-stacked graphene. The percentage of tri-layer GNRs is very low compared with single and bi-layer ones, so we had few Raman data of tri-layer GNRs. The positions and FWHM of 2D band for single, AB-stacked bi- and ABA-stacked tri-layer GNRs were recorded in Table S1. The up-shift and broadening of the 2D band was consistent with AB-stacked graphene sheet. We also measured the low frequency region (100-300 cm^{-1}) of GNRs and never observed the radial breathing mode (RBM) which is intrinsic to CNTs. A small peak at ~1440 cm^{-1} was observed in Raman spectra of GNRs. Control experiments found that this peak was attributed to trace PMMA left on SiO_2 after transferring GNRs (Fig. S4). Figure S5 showed a typical Raman spectrum of a bi-layer GNR obtained by lithographic etching of pristine-graphene sheets. Compared with GNRs produced by our approach, the I_D/I_G of lithographic patterned GNR was high (~2.0) and the 2D peak was broader (~90 cm^{-1}), suggesting the quality of our GNRs was higher than lithographically patterned ones.

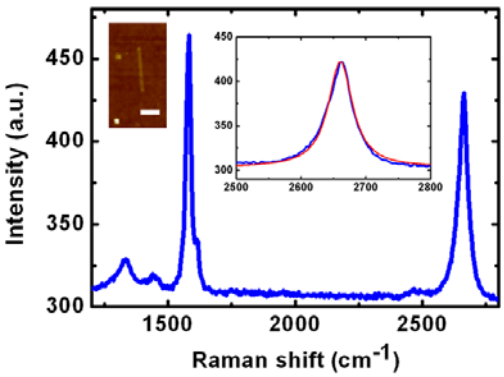

Figure S2 Raman spectrum of a non-AB-stacked bi-layer GNR. Left inset: AFM image of the GNR. Scale bar: 100 nm. The width and height of the GNR are 25 nm and 1.4 nm, respectively. The height of the GNR is similar to other bi-layer GNRs with AB stacking. Right inset, 2D band peak (blue) and the best fit curve (red) as a single Lorentzian expected for non-AB stacked bi-layer GNR.

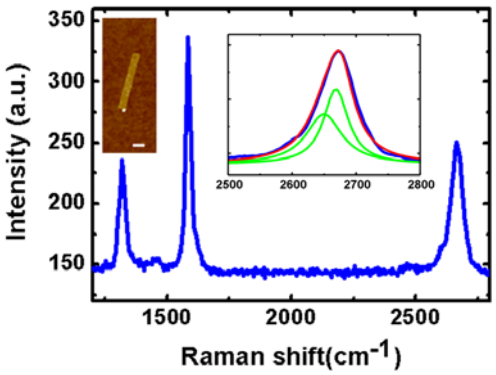

Figure S3 Raman spectrum of a tri-layer GNR shown in the left inset. Scale bar, 100 nm. Right inset, 2D band spectrum (blue) and the best fitted curve (red) with two Lorentzian peaks (green).

Table S1 The 2D band positions and FWHM for GNRs with different number of layers.

Number of layers	2D band position (cm^{-1})	2D band FWHM (cm^{-1})
1	2659	38
2	2665	54
3	2673	60

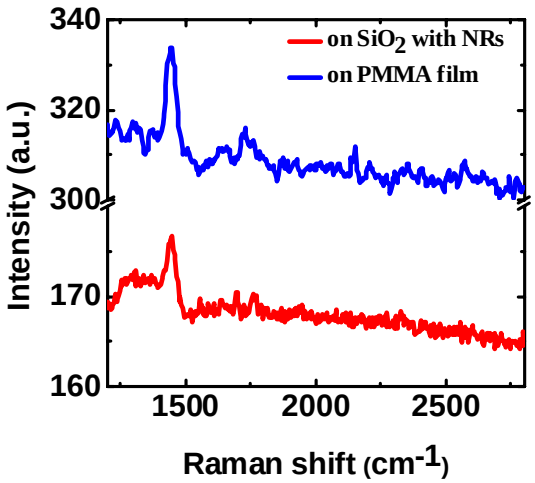

Figure S4 Raman spectra of SiO_2 substrate with transferred GNRs (red) and PMMA film (blue).

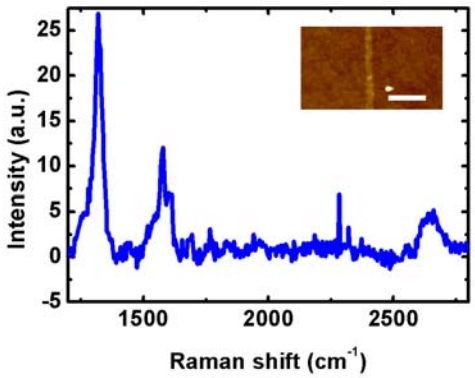

Figure S5 Raman spectrum of a bi-layer GNR (~28 nm wide) obtained by lithographically etching of pristine-graphene sheets. Inset is the AFM image of the GNR, scale bar: 200nm.

(4) Raman spectra of pristine MWNTs

Because MWNTs contain an ensemble of CNTs with diameters ranging from small to very large, the Raman spectra of MWNTs are complex and each MWNT show Raman spectrum with different lineshape[1]. Figure S6 showed two typical Raman spectra of individual MWNTs. 2D band was observed on some MWNTs and could be fitted with multiple peaks. The 2D band width of MWNTs (>60 cm^{-1}) was broader compared with single-walled carbon nanotube (~25 cm^{-1}), single (~40 cm^{-1}) and bi-layer GNRs (~55 cm^{-1}). No obvious D band was observed on all the MWNTs, which indicated the high quality of the raw materials.

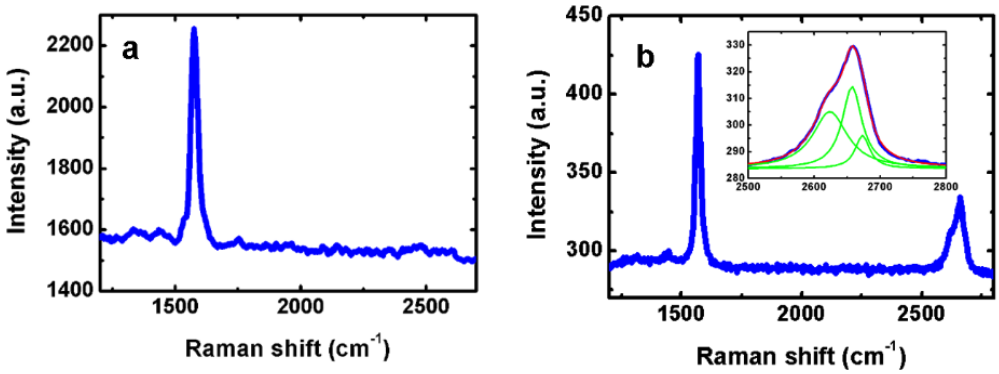

Figure S6 Raman spectra of pristine MWNTs on SiO_2/Si substrate. **a**, Raman spectrum

of a MWNT without 2D band. **b**, Raman spectrum of a MWNT with 2D band. Inset, 2D band spectrum (blue) and the best-fit curve (red) with three Lorentzians (green).

(5) Choice of plasma source and etching parameters

O_2 plasma etching of CNTs was isotropic even with the partial protection of PMMA. The height difference along the same MWNT (Fig. S7) indicated the removal of the shells of MWNT by O_2 plasma. The height difference of the two sections along the MWNT was ~ 0.8 nm, corresponding to one or two shells. To find out the optimized etching time, we tested different etching times. Figure S8a, b and c showed the AFM images of GNRs generated by etching for 20 s, 20 s and 30 s, respectively. The Raman spectrum of a GNR obtained by etching for 30 s was shown in Fig. S8d.

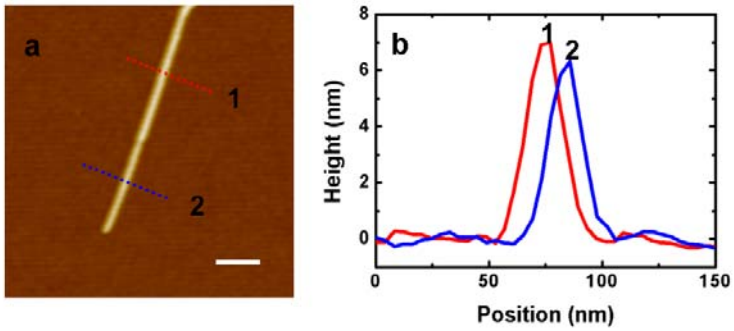

Figure S7 a, AFM image of a MWNT after etching by O_2 plasma. **b**, Cross sections of MWNT along line 1 and 2.

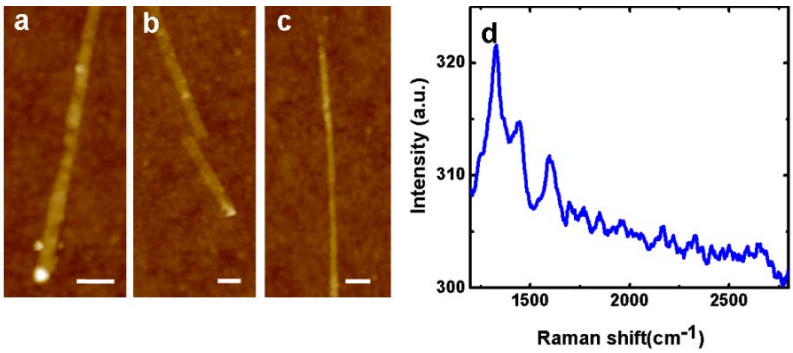

Figure S8 a and **b**, AFM images of GNRs obtained by etching for 20 s. **c** and **d**, AFM image and Raman spectrum of a GNR obtained by etching for 30 s.

(6) Transfer properties of more GNR device

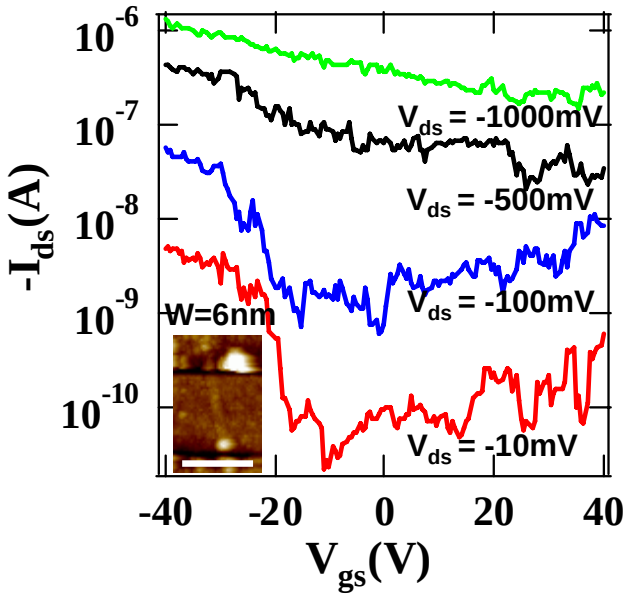

Figure S9 Current-voltage I_{ds}-V_{gs} curves for a ~6 nm wide GNR device at various bias when probed in air (inset is the AFM image, scale bar is 200 nm). It has an $I_{on}/I_{off} > 10^2$.

We probed the device shown in Figure 4b in air, in vacuum and after electrical annealing in vacuum (Fig. S10). The Dirac point moved to around V_{gs} ~ 0 V after electrical annealing by removing physisorbed O_2 and other p-doping sources. The conductance at the Dirac point remained similar before and after electrical annealing. This suggested similar quality/crystallinity of the GNRs before and after electrical annealing, which also indicated the high quality of the as made ribbons.

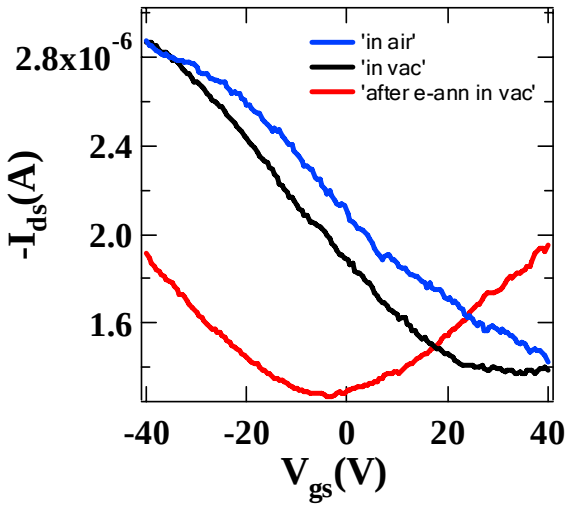

Figure S10 The Current-voltage I_{ds}-V_{gs} curves of the device shown in Figure 4b probed in air (blue curve), in vacuum (black curve) and after electrical annealing by applying electrical bias of up to 3V (red curve).

Reference

1. Dresselhaus, M. S., Dresselhaus, G., Saito, R. & Jorio, A. Raman spectroscopy of carbon nanotubes. *Physics Reports* **409**, 47-99 (2004).
2. Hass, J. *et al.* Why multilayer graphene on 4*H*-SiC_(0001) behaves like a single sheet of graphene. *Phys. Rev. Lett.* **100,** 125504 (2008).
3. Faugeras, C. *et al.* Few-layer graphene on SiC, pyrolitic graphite, and graphene: A Raman scattering study. *Appl. Phys. Lett.* **92**, 011914 (2008).
4. Campos-Delgado, J. *et al.* Bulk production of a new form of sp^2 carbon: crystalline graphene nanoribbons. *Nano Lett.* **8**, 2773-2778 (2008).